10

Laser-Driven Radiation Therapy

Dietrich Habs[1], Toshiki Tajima[2] and Ulli Köster[3]
[1]*Max Planck Inst. for Quantum Optics, Garching*
Faculty of Physics, LMU Munich
[2]*Faculty of Physics, LMU Munich*
[3]*Institute Laue-Langevin, Grenoble*
[1,2]*Germany*
[3]*France*

1. Introduction

A class of novel cancer treatment methods in radiation therapy using intense lasers has been investigated and developed in recent years. We review the latest status and future prospects in this field. Radiation therapy is playing an ever increasing role in the treatment of cancer and other illnesses, compared to other treatment options, it shows a good response with acceptable side effects for the patient and a good cost-benefit ratio.
Radiation therapy comes in different variants, mainly *external beam radiation therapy (EBRT)*, where the radiation sources are positioned outside the patient, and *endoradiation therapy*, where sealed radiation sources are positioned in the treatment zone, or *systemic radionuclide therapy*, where unsealed radionuclides are injected into the patient's body.
EBRT can be performed with X-rays, gamma-rays, electrons, neutrons or ion beams. Ion beams (such as proton and carbon beams Tajima (2009)) have the distinct advantage in reducing unwanted radiation dose on healthy tissues before and behind the tumor region due to the Bragg peak. On the other hand, the physical installation (accelerator, gantry, and radioprotection measures) for ion beams is larger and more costly. Laser-driven ion beams are small and lend themselves also for the treatment of smaller tumors. For this purpose, a new dose monitoring method is introduced, namely on-line monitoring of laser-driven ion beams via prompt gamma ray detection.
Endoradiation therapy too can profit from advanced laser technology and laser applications. Here laser-driven γ beams are produced by Compton backscattering of laser light from relativistic electron beams. They are nearly monoenergetic and have a low divergence and high brilliance. Compared to present day γ beams, new beams with much higher flux and much better monochromaticity become available, using new techniques of intensified interaction between laser and electron beam. Due to their much smaller opening angle they allow focusing with refractive γ lens optics for the first time, opening a new world of *nuclear photonics*. These γ beams can be employed to induce photonuclear reactions to selectively generate new radioisotopes or nuclear isomers with high specific activity Habs (2011). With conventional methods, such radionuclides cannot be produced in the required quality or quantity, but they will become available with γ beams. Thus, e.g., in many cases "matched" pairs of isotopes of the same element become available, one for therapy and one for diagnostics, allowing for an optimized therapy. Some new isotopes kill the cancer cells

due to the short-range interaction only in a small volume, making a very localized treatment possible. This will be outlined in detail in Section 3 of this chapter.
We present here one possible school of thought for these goals based on an oncological consideration. This idea is based on the following observation Abe (2007); Molls (2009). Dr. Molls argues: "In chemotherapy the tumor cell kill depends on the transport of the substance to the clonogenic cells and molecular targets, DNA repair capacity, repopulation, pO_2, pH, etc. In macroscopic tumors not all the subvolumes of the tumor, clonogenic cells and relevant molecular targets are reached by those doses of the medical substance which are needed for cell kill. In other words," he goes on, "the chemotherapy dose distribution is intrinsically inhomogeneous." On the other hand, Dr. Molls points out, "In radiation therapy the tumor cell kill depends on intrinsic radiation sensitivity, DNA repair capacity, repopulation, oxygenation status etc. However, the entire tumor can be irradiated matched with the dose, which is necessary to kill all clonogenic tumor cells, even the most resistant ones." In other words, "it delivers a matched dose distribution," citing the superior feature of radiation therapy.
The process in the detection of small and even micro tumors by such methods as phase contrast imaging Pfeiffer (2006) gives us hope for such a vision. Such techniques point us towards small (or even micro) tumor detection. For proton laser-driven (or ion) beam radiotherapy, the therapy of small tumors is well suited.

2. Laser-driven ion therapy

2.1 New trends in ion acceleration

It is important to improve the laser ion interaction in both its energy and the quality of the beam. The progress in recent years makes us hopeful. Energetic proton and ion beams with high beam quality, such as quasi-monoenergetic spectra, have been produced in the last few years from thick metallic foils (e. g. μm thick aluminum) irradiated by ultra intense short laser pulses with appropriate target preparations Hegelich (2006); Schwoerer (2006); Snavely (2000); Ter-Avetisyan (2006). Most previous experiments fall in the regime called TNSA (Target Normal Sheath Acceleration) using what we regard as relatively thick targets (($\sim \mu$m) Fig. 1). In this regime electrons are first accelerated by the impinging intense laser pulse and penetrate the target. Leaving the target at the rear side, the electrons set up an electrostatic field that is normal to the rear surface of the target. Ions accelerated from solids originate primarily from contaminant layers of water vapor and hydrocarbons on the target surface. As these targets are thick, the laser pulse is mostly reflected and the conversion efficiency of laser energy to ion energy is normally less than 1 %, the maximum energy scales with less than a linear function of the laser intensity. The maximum proton energy based on the TNSA mechanism has not improved since 2000 ($\sim$ 60 MeV). As reviewed by Robson et al. Robson (2007) (in particular their Fig. 1a), their fit of the data experimentally obtained (what they collected are all TNSA) shows that ion energies are proportional to the square root of the laser intensity I_L, which is proportional to a_0^2, where the dimensionless normalized vector potential a_0 is defined as: $a_0 = \frac{e\,E_L}{m_e c\,\omega_L} = \left(\frac{I_L\,[\mathrm{W\,cm^{-2}}]\cdot\lambda_L^2\,[\mu\,\mathrm{m}^2]}{1.37\cdot 10^{18}}\right)^{1/2}$, where m_e is the electron mass and ω_L the laser frequency. In TNSA, the laser energy is absorbed at the front surface of a solid target. Hot electrons are generated by a variety of mechanisms. Since electrons gain kinetic energy through interaction with the laser, typically up to the ponderomotive potential

$$\varepsilon_0 \approx e\Phi = m_e\,c^2\left(\sqrt{1+a_0^2}-1\right)\,, \tag{1}$$

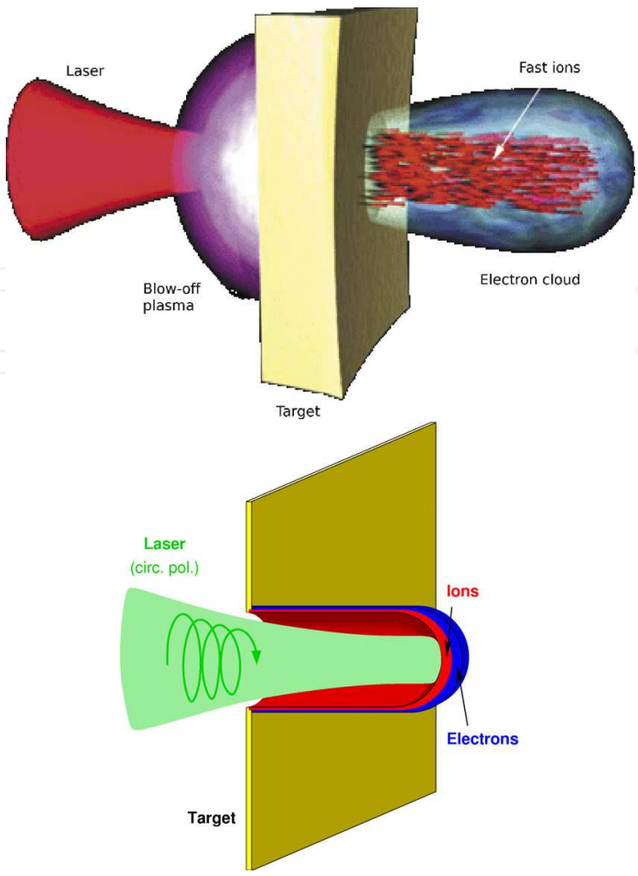

Fig. 1. Schematic picture of "Target Normal Sheath Acceleration" (TNSA, left)Wilks (2001) and Coherent Acceleration of Ions by Laser (CAIL, right), in particular Radiation Pressure Acceleration (RPA). The dynamics of electrons remains coherently slaving to the laser fields, in sharp contrast to TNSA Tajima (2009).

the electron energy gain is approximately proportional to a_0, when a_0 is much greater than unity (which is the case for the data analyzed). Then through certain mechanisms the heated electrons transmit their energy to ions, which is again thus proportional to a_0.

In the present review, however, we would like to report the progress that now emerges with a new class of experiments and theory that supports such experiments, in which a regime of much more efficient and possibly higher energy acceleration processes exists. We will scrutinize the process of this energy transfer between electrons and ions, both for TNSA and the new regime that we now describe as Coherent Acceleration of Ions by Laser (CAIL), i. e. a regime of interaction more direct than TNSA. However, it is worthwhile to look at one aspect of the laser interaction with electrons. At higher laser intensities above 10^{22} W/cm^2, numerical simulations seem to indicate that a laser could also accelerate protons to high energies Bulanov (2009). With a compact high-repetition laser system, however, the highest proton energy is still lower than 20 MeV in all experiments Fuchs (2006). In order to realize 200 MeV/u beams for proton/ion therapy, the laser intensity required should be as high as 10^{22} W/cm^2 Fuchs (2006).

Experiments, producing high-energy ions with sub-micrometer to nanometer thick targets that are much thinner than those used so far, have shown far superior acceleration

characteristics Henig (2009) and have recently attracted strong interest. A typical physical situation is depicted in the sketch in Fig. 1. With the emerging nanometer target of diamond-like carbon (DLC), the conversion efficiencies are one to two orders of magnitude higher ($> 10\,\%$) even with modest-energy lasers (less than 1 Joule per pulse, and highly repetitive lasers) compared with those in the regime of TNSA with the thicker targets, and so the laser pulse can accelerate the ions to higher energies. The experiments show that the proton energy increases as the target thickness decreases for a given laser intensity, and that there is an optimum thickness of the target (several nm) at which the maximum proton energy peaks and below which the proton energy now decreases.
This optimum thickness for the peak proton energy is consistent with the thickness dictated by the relation Esirkepov (2006); Liu (2008); Matsukado (2003); Rykovanov (2008)

$$a_0 \sim \sigma = \frac{n_0\, d}{n_c\, \lambda_L}, \tag{2}$$

where σ is the (dimensionless) normalized electron areal density, n_0 the electron density of the target, and n_c is the critical density. Note that this optimum thickness for typically available laser intensities is much smaller than the previously attempted target thicknesses (for ion acceleration). Thus we attribute the observed singularly large value of the maximum proton energy in the recent experiments Steinke (2010; 2011) to the ability to identify and provide prepared thin targets of the order of nm to reach this optimum condition. In reality, at this target thickness the laser field comes to the point of partial penetration of the target, rendering the realization of optimum rather sensitive. The experiments show that transparency plays an important role in energy enhancement. As we shall show, in this new regime (CAIL) with σ/a_0 of the order of unity (as opposed to $\sigma/a_0 \gg 1$ in TNSA), the electron dynamics remains coherent, directly following the laser field. Thus we call this regime of acceleration Coherent Acceleration of Ions by Laser (CAIL).

2.2 How ions are accelerated with laser and electrons

The characteristics of the previous laser ion acceleration experiments (TNSA) are that (i) laser ion acceleration has great potential, particularly in its accelerating gradient (of the order of TeV/m) and thus compactness of acceleration; (ii) however, its progress has lagged since the initial observation Clarke (2000); Maksimchuck (2000); Snavely (2000) in 2000 in enhancing its energy and other aspects with less energy laser drive, often limited to several MeV energy gain Fuchs (2006); Robson (2007); (iii) further, the energy spectra of ions remain broad Fuchs (2006), except in exceptional cases Hegelich (2006); Schwoerer (2006); Ter-Avetisyan (2006); and (iv) the efficiency remains low Fuchs (2006). On the other hand, although the numbers achieved are so far not overwhelming, some reports indicate one or two possible ways out, when, for example, the plasma density is near the critical value Matsukado (2003); Yogo (2007).
The above situation may be broadly summarized as follows. The intense laser somehow heats electrons of the solid target to high energies, which contributes to a large space charge separation on a rapid time scale of electron runaway from the surface of the target (the rear surface), which pulls ions and makes them run after the escaped electrons. The electron heating involves complex processes, both coherent and individual particle processes (such as collisions), and the original electron motion in the intense laser field is cascaded down to a thermal spectrum of electrons that drive ions as described above. Firstly, this means that the electron spectrum is broadly spread (such as Maxwellian) and is certainly limited to or less than the ponderomotively driven electron energy of $m_e c^2 \sqrt{1 + a_0^2}$. The scaling to the intensity

of the laser never greatly exceeds $\sqrt{I_L}$, as shown in the limiting energy of electrons McKenna (2007); Robson (2007). Secondly, hot electrons suddenly escape from the target, so that the ions are unable to follow the electrons with the result that some fraction of these electrons run away from the ions and the rest of them are pulled back toward the ions. The ions are unable to be smoothly accelerated; in other words, the gradual (adiabatic) acceleration process is nonexistent. This non-adiabatic nature of the ion dynamics is the underlying reason for exhibiting properties (ii) – (iv). These features arise essentially from the mismatch between the group velocity of photons and the velocity of electrons subsequently energized and that of the ions. The ions remain slow and non-relativistic, while photons and electrons are relativistic.
Thus, our principal direction is first to utilize the photon energy more directly rather than cascading through multiples of collisional processes, and secondly to transfer laser energy to electron energy and to ions more adiabatically. When the solid target is too thick, most ions remain stationary and the momenta of photons are spread over broadly. Thus we should limit the number of ions influenced by laser acceleration. Secondly, in order that the twofold interaction process of laser to electrons and from electrons to ions becomes more gradual, we need to slow down the photons and electrons and make them match the sluggish ions, at least initially, until they reach high speed Mako (1984). Laser electron acceleration Tajima (1979) may be easier in this sense, because light electrons at rest may be more easily trapped by the speeding photon-driven waves, whose velocity is near c, whereas the trapping velocity width Esaray (1995) is $\sqrt{e\Phi/m_e} \sim c$, where Φ is the ponderomotive potential. This ponderomotive potential is capable of inducing the wakefield with amplitude of the order of $E_w \sim m_e\omega_p\, c/e$. This is why in the laser electron acceleration the fast wakefield $v_{\rm gr} \sim c$ can still trap stationary electrons ("self-injection"). Meanwhile for ions $\sqrt{e\Phi/m_i} \ll c$, and this value can only become $\sim c$, when $a_0 = \mathcal{O}(m_i/m_e)$ (ultrarelativistic), where m_i is the mass of ions. More importantly, in order to trap ions, the trapping velocity width of ions is much smaller than that for electrons

$$v_{i,\rm tr} \sim \sqrt{\frac{m_e}{m_i}\, a_0\, Q}\, c\ , \tag{3}$$

where Q is the ion charge in units of e (electron charge). Thus, in the regime of our interest $1 \leq a_0 \ll m_i/m_e$ the accelerating structure has to move at a velocity within this $v_{i,tr} \ll c$. For ions to obtain net energy gain, the ion velocity needs to be within the trapping separatrix, which is situated over the velocity band that is centered at the phase velocity $v_{\rm ph}$ of the accelerating structure (we will call it a "bucket" later in Sec. 2.4.3) with a trapping width $v_{i,\rm tr}$. Ions outside of this band (either above or below) simply oscillate in energy, but obtain no net energy gain. Even when the bucket velocity $v_{\rm ph}$ increases in time, ions that are trapped deeply enough may be kept trapped and, therefore, continue to gain energy from the bucket. This is the principle of gradual acceleration. Either when the velocity $v_{\rm ph}$ increases too suddenly or when ions are outside of the trapping separatrix, ions spill out or are left out of the accelerating structure.
In order to accomplish the first goal, one way is to adopt a very thin foil so that the mass contained in this foil is tiny. Alternatively, a diluter medium such as a dense gas or matter with clusters could be used. In order to accomplish the second goal, the most direct way to do so is to choose the density of the target material to result in a vanishing group velocity of photons such that ions can respond adiabatically. In this regard, it further helps if we can control the velocity of the accelerating structure to match the accelerated ion velocity. These considerations lead us to consider to look at very thin foil targets and alternatively at matter at or close to the critical density.

Another consequence of this general consideration entails a strategy to slow down the electron motion after they are emitted from the target. This may be done by providing a concave geometry of the surface Tajima (2005) or other target preparations. One of the recent hopes is to employ circularly polarized laser pulses (CP). These, unlike the linearly polarized laser pulses, do not have sudden high frequency ($2\omega_L$) motions by linearly polarized photons, but only result in a smooth ponderomotive acceleration of the target Klimo (2009); Macchi (2005); Qiao (2009); Robinson (2008); Rykovanov (2008). If the CP ideally works, the ponderomotive force on electrons induces and matches the electrostatic force generated between the charge separated ions and electrons, and this keeps the overall dynamics smooth and adiabatic. A somewhat extreme and earlier rendition of this concept may be that of the radiation dominant acceleration by Ashour-Abdalla et al. Ashour-Abdalla (1981) and Esirkepov et al. Esirkepov (2004), where the laser photon pressure drives electrons to relativistic speed that drags ions also to relativistic speed closely following the electrons.

2.3 CAIL and RPA experiments

In this section we present recent experimental progress on laser ion acceleration, which shows marked improvements over experiments in the regime of TNSA: in (i) the total conversion efficiency of laser energy into ion energy, (ii) the maximum observed ion energies, and (iii) the production of monoenergetic peaks in the ion energy spectra. We compare these results to previous experiments, which are based on the TNSA mechanism, established over the last 10 years in experimental and theoretical efforts. In TNSA one has observed for certain laser parameters, e.g. 1 PW lasers with 500 fs, maximum conversion efficiencies of 12 %, or one has observed maximum proton energies of 58 MeV Snavely (2000) and by filtering out small target regions could produce quasi-monoenergetic ion spectra Hegelich (2006); Schwoerer (2006); Ter-Avetisyan (2006). At present, similar experimental values of efficiency, energy, etc. can be obtained with much smaller lasers. The formerly predicted laser parameters based on TNSA Robson (2007) to reach ion energies of 240 MeV for protons or 450 MeV/u for carbon ions for medical therapy facilities have been rather big and the laser would end up costly. The new regime, where coherent dynamics of electrons in accelerating ions by laser (CAIL) plays a significant role, can yield scaling laws that lend to a prospect that short-pulse, high-intensity lasers with high repetition rate may drive ion beams competitive with classical radio-frequency accelerator systems.

2.3.1 Laser ion acceleration with ultra-thin foils (CAIL)

In order to realize the CAIL regime, one wishes to employ nanometer thick target foils together with high-intensity short pulse lasers. In search of ultra-thin free standing foils that withstand strong ion and electron bombardment, DLC foils appear to be eminently suited. They have a very high tensile strength, large hardness, good heat conduction, high heat resistance and, when used as stripper foils, they show a large survival rate for ion bombardment. With a special production technique free-standing foils with 75 % sp^3 bonds – diamond-like bonds – can be produced.

The thickness of the DLC-foils has been characterized by means of an atomic force microscope (AFM) with an accuracy close to 0.5 nm Tajima (2009). Furthermore, the detailed depth composition – showing also front layer contaminations – was measured via Elastic Recoil Detection Analysis (ERDA)Tajima (2009).

A second ingredient in these laser acceleration experiments Henig (2009); Steinke (2010) is an ultra-high contrast of the laser pulses to avoid the preheating and expansion of the target before the interaction with the main laser pulse. The intensity of prepulses and the amplified

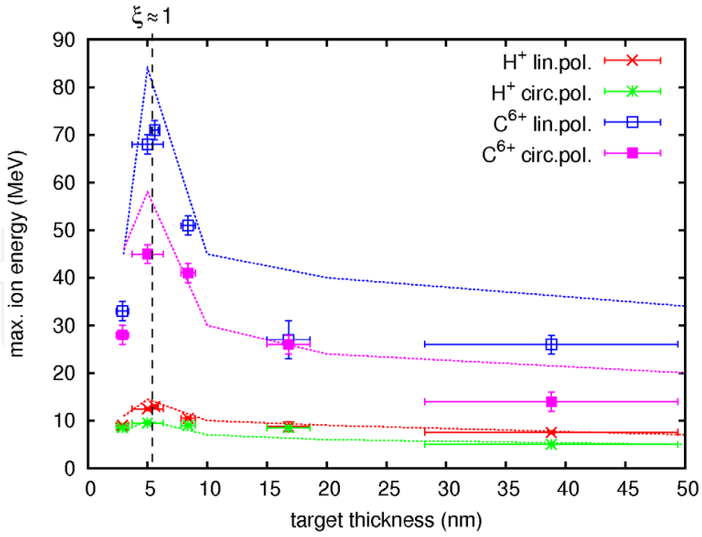

Fig. 2. Maximum cutoff ion energies as a function of target thickness in the regime of CAIL experiments Henig (2009). Theoretical curves are from the CAIL theory. Observed values and theory (CAIL) are in good agreement over a broad parameter range. The optimum condition is realized at a thickness parameter $\sigma \approx a_0$ Tajima (2009).

spontaneous emission (ASE) pedestal are characterized with a 3rd order auto correlator, yielding typical values of 10^{-7} at 10 ps before the main pulse. This value was further improved by a recollimating double plasma mirror, which lets the low intensity prepulse pass through, while it reflects the high intensity part of the pulse. In this way an estimated contrast of $\sim 10^{-11}$ was achieved. For the longer laser pulses the contrast was improved by Self-Pumped Optical Parametric Amplification (SPOPA) Shah (2009), using nonlinear optical effects and thus avoiding the 50 % energy loss of the double plasma mirror.
Ultra-thin foils in two regimes have been investigated so far: (i) for laser pulses of 45 fs duration at the laser of the Max-Born Institute (MBI) in Berlin and (ii) for laser pulses with 700 fs duration at the Trident laser in Los Alamos. Laser accelerated ions were measured with a Thomson parabola spectrometer.

2.3.2 Characteristics with ultra-thin targets

Let us now discuss jointly all results for ultra-thin targets in comparison to the thicker targets results, where TNSA is the dominant acceleration mechanism.
In Fig. 3 we compare the conversion efficiency from laser energy to ion energy. At the optimum target thickness and 45 fs laser pulses, an optimum conversion efficiency of 10 % for laser energy into ion energy was obtained by integrating all protons above 2 MeV and all carbon ions above 5 MeV for the linearly polarized laser. Correspondingly, $\sim$ 9 % was obtained for circular polarization. For the 700 fs experiment a lower efficiency of about 2 % was observed. The values are shown in Fig. 3 in the comparison of the CAIL results with efficiencies for thicker foil targets (TNSA). We show the general trends of the TNSA mechanism by theoretical results from the fluid model Fuchs (2006), which describes the experimental data quite well. In addition, we show specific experimental results for the ASTRA laser Spencer (2003), the RAL PW laser McKenna (2004) and the NOVA PW laser Snavely (2000). We observe approximately a 50 fold increase in conversion efficiency for thin targets with the 45 fs pulses compared to TNSA at the same laser intensity, also taking our

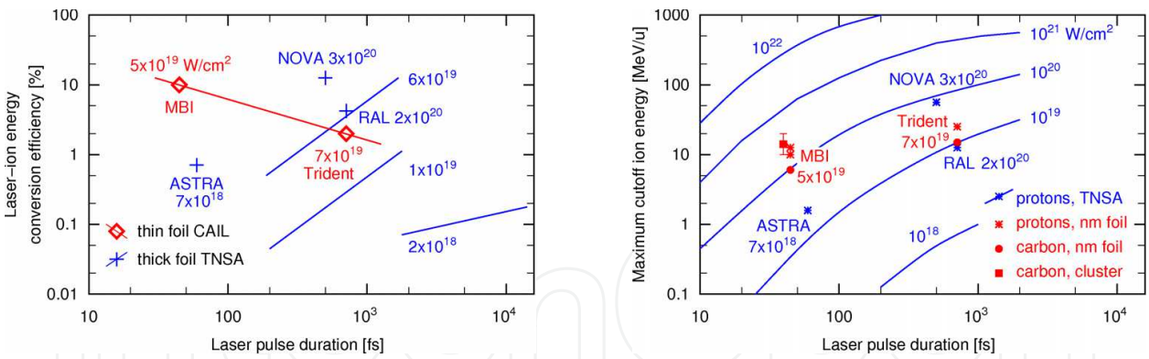

Fig. 3. Left: Conversion efficiency of laser energy to ion energy comparing results from thick targets and the TNSA mechanism to measurements with ultra-thin targets in the regime of CAIL (red diamonds and line). For the TNSA mechanism smooth curves from the fluid model by J. Fuchs Fuchs (2006) are shown together with some experimental points: ASTRA Spencer (2003), NOVA Snavely (2000), RAL McKenna (2004). Right: Maximum cutoff energies of ions given in MeV/u as a function of laser pulse duration. The energy gain by CAIL experiments is embedded with red dots in the predicted curves of TNSA. Note that in shorter pulses, energies by CAIL are more than an order of magnitude higher than for TNSA. Here also the results from the cluster target of Sec. 3.1.3 are shown Tajima (2009).

own measurements at larger target thicknesses into account. For 700 fs pulse duration the efficiencies of thick target TNSA results and thin target results are comparable. If one increases the pulse duration, for short pulses the optimum target areal electron density $\sigma \approx a_0$, while for longer pulses σ has to be significantly larger to reach the maximum cutoff energy. Here one first has to reach the relativistic transparency of the target by expanding the target (see Sec. 2.4.2), explaining in part the reduced conversion efficiency. For somewhat shorter laser pulses and cold adiabatic RPA, a 60 % conversion efficiency has been predicted theoretically for higher laser intensities in an idealized 1D PIC simulation Robinson (2008). Experimentally, the optimum conditions depend on many parameters such as optimum laser focusing to prevent heating of the walls of the bulged out target Klimo (2009).
In Fig. 3 we compare the maximum cutoff ion energy for protons and carbon ions between measurements with ultra-thin targets and μm thick targets, where the TNSA mechanism dominates. In Fig. 3 for TNSA only proton energies are shown for model calculations, which reproduce the experiments quite well Fuchs (2006). Approximately an increase by a factor of 10 is observed for the short laser pulses of 45 fs in the cutoff energies between TNSA and CAIL. An overall increase in energy occurs for both processes for longer laser pulses. At the PW level the proton energies for TNSA vary from 58 MeV Snavely (2000) to 13 MeV McKenna (2004) for similar pulse energies of 500 J and 400 J. Thus it is difficult to obtain a good comparison with the results of ultra-thin targets. For the carbon ions and the longer pulse of 700 fs, a factor of 4 higher energies were observed for a factor of 4 smaller pulse energies, pointing to a clear advantage of the ultra-thin targets in CAIL. For the short pulses of 45 fs again an order of magnitude improvement is seen for the ultra-thin targets (CAIL).

2.3.3 Cluster target experiments

Fukuda et al. Fukuda (2009) explored a different path of laser ion acceleration for hadron therapy: They use a gas jet target mixed with submicron clusters. The target consists of a He gas jet with a density of $1.5 \cdot 10^{19}$ cm^{-3}, into which solid-density CO_2 clusters with an average diameter of several 100 nm are dispersed at a cluster density of $3 \cdot 10^9$ cm^{-3}. This constitutes

an average density at or near the critical density. A well-formed self-channeling phenomenon coincides with the detection of high energy ions. They observe in their ion spectrometers rather high ion energies in the range of $10 - 20$ MeV/u for carbon, oxygen, or helium ions with a small divergence angle of 3° Fukuda (2009; 2011). This maximum energy value is much higher than expected from TNSA.
It is noted that the average density near the critical density may have played an important role, perhaps similarly to Matsukado et al. Matsukado (2003) and Yogo et al. Yogo (2007). In these experiments the enhancement of ion energies was noted when the density is in the neighborhood of the critical value. Thus the acceleration with clusters has commonality with the dynamics observed in the long pulsed thin target (Sec. 2.4.2) after the laser burns through the target (see also Sec. 2.4.2), when the density becomes critical through relativistic transparency. Near the critical density, as we noted, the group velocity of photons is small. In recent simulations Kishimoto (2009) the maximum ion energy is observed to scale with the pulse length, with the intensity fixed, and inversely proportional to the size of the clusters. Thus the nano-structured targets may provide an enhanced coupling of laser and ions Kishimoto (2000). Higher efficiencies may be obtained by increasing the pulse energy, the contrast of the laser and using much smaller clusters with higher density.
Recently, ion acceleration up to 50 ± 25 MeV/u has been achieved using the cluster-gas target with the 20 TW (40 fs, 800 mJ) J-KAREN laser system Fukuda (2010) and five times more power than the earlier experiment. If we combine the two experimental results, an extrapolation shows that a 100 TW-class Ti:Sa laser is capable to generate 200 MeV/u ions. In addition, particle-in-cell simulations have delivered an energy scaling of ions generated by the magnetic vortex acceleration in near-critical density plasmas Nakamura (2010), providing a possible acceleration mechanism for the cluster-gas targets. The scaling suggests that a 100 TW-class laser is capable to generate 200 MeV protons, consistent with the experiments.
Therefore, both experiments and theory predict that 100-TW class Ti:Sa lasers, which are achievable using the present laser technologies, reach the ballpark of 200 MeV ions applicable to medical use. Such experiments will be conducted in the near future.

2.4 Towards more efficient and gradual acceleration

have been motivated by much thicker the TNSA regime electrons are first accelerated impinging relativistic laser pulse and they penetrate the target target at the rear side, field that points normal to was the origin of the terminology of the TNSA Most electrons are forced to turn around quasi-stationary assumed to follow a thermal studies of the conventional
Most of the theories for thicker targets are based on TNSA Andreev (2008); Ceccotti (2002); Mora (2003; 2005); Passoni (2004; 2008). Though this mechanism is widely used in the interpretation of the experimental results, it does not apply to the ultrathin nanometer scale targets because the direct laser field and partially transmitted laser pulse play an important role in electron dynamics and the energetic electrons oscillate coherently, instead of showing chaotic thermal motion. In order to design a compact accelerator with a modestly intense laser for medical applications we discuss here, it is desirable to understand the new emerging regime that is promising for this purpose.

2.4.1 Efficient energy gain in the CAIL regime

In case of a thin target, electron motions maintain primarily those organized characteristics directly influenced by the laser field in the CAIL regime, rather than chaotic and thermal motions of electrons resulting from laser heating on the front surface, where the laser is either absorbed or reflected for the TNSA regime.

It may be instructive to compare conceptual differences of the regime of TNSA and that of CAIL. See Ref Tajima (2009) for details. In the TNSA case the laser interacts primarily at the front surface of the target, while in all cases of the CAIL interaction takes place at the rear surface. In the regime of TNSA electrons that have gained energy at or near the front surface propagate through the target and escape from the rear surface with a broad energy spread. In a model problem Mako (1984); Tajima (1978) in which the electron beam (with a delta-function energy spectrum) enters from the metallic surface that may be regarded as the rear surface, the energy gain was analyzed. In CAIL, once the laser penetrates the target and electrons gain energy from the laser, the electron dynamics in the presence of the rear surface is once again similar to this process.
In an ultra-thin target, the laser electromagnetic fields largely sustain coherent motions of electrons. As partially or fully penetrated laser fields in addition to the laser fields in the target, the electron motion under laser fields is intact and is characterized by the transverse field. The electron energy consists of two contributions, the kinetic energy of (organized) electrons under the laser and the ponderomotive potential of the partially penetrated laser fields that help sustain the electron forward momentum. Following the analysis of Ref. Mako (1984); Tajima (2009), the maximum ion energy is

$$\varepsilon_{\max,i} = (2\alpha + 1)\, Q\, \varepsilon_0, \tag{4}$$

where ε_0 is given by Eq. (1). The enhancement of the ion energy gain in Eq. (4) in the CAIL is due to the factor $(2\alpha + 1)$ compared with the equivalent TNSA energy gain Eq. (1). In Eq.(4) we see that the ion energy is greater if the coherence parameter of electrons α is greater: (a) the energy gain of the present case is several times higher than that of TNSA; (b) the energy gain maximizes at the optimum thickness of $\sigma \approx a_0$ mentioned earlier in Sec. 2.1 for CAIL, as opposed in a much thicker target for TNSA. These features are also seen in Fig. 4 later.

2.4.2 Relativistic transparency

Understanding the dynamics of the laser pulse and the target evolution is important when the pulse is longer ($\sim$ hundreds of fs) than tens of fs and / or the target is thicker than a few nm. We now consider the cases when the target is thicker ($(\sigma/a_0) \gg 1$) than when it is immediately influenced by the laser fields, but still σ/a_0 is less than for TNSA. In this case the laser does not immediately penetrate through the target. We can delineate at least three stages. The first stage is similar to the situation we described above for $\sigma \approx a_0$. The laser just impinges on the thin surface layer of the dense target. The second stage starts when the target begins to expand by the laser interaction, primarily in the direction of laser propagation until the plasma becomes relativistically transparent at time t_1. After this relativistic transparency time t_1, the plasma expands in all three dimensions. The third stage begins when the plasma becomes underdense at time t_2 (the classical transparency time) and lasts until the pulse is over.
One of the distinguishing features of the thin target CAIL regime, as compared with TNSA, is the presence of the relativistic transparency time t_1 before the pulse length τ, so that the laser pulse emerges or interacts with the entire target before the pulse is gone. We find this time to be Yan (2009a)

$$t_1 \cong \left(\frac{12}{\pi^2}\right)^{1/4} \frac{N^{1/2}}{a_0^{1/2}} \left(\tau d/C_s\right)^{1/2}. \tag{5}$$

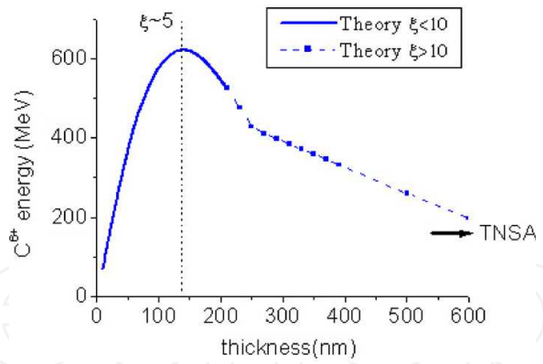

Fig. 4. The maximum ion energy driven by the laser pulse as a function of target thickness in the regime of CAIL. The optimum is reached at $\xi = (\sigma/a_0) \sim 5$. Energies for thicker targets decrease from this value, eventually leading to the value often found in the TNSA regime (μm or more in this graph). C^{6+} energy gain estimated from Eq.(7) as a function of target thickness and with $\alpha \cong 3$. (For a given laser pulse length at 700 fs and laser amplitude $a_0 = 20$). The contribution of the electron energy gain after the relativistic transparency has been reached is dominant Tajima (2009). The experimental points by Hegelich et al., Hegelich (2011) closely follow the theoretical prediction

Here the sound speed $C_s \cong (Qm_e c^2 a_0/m_i)^{1/2}$ and $N = n_0/n_c$. The relativistic transparency time t_1 in Eq.(5) is approximately the geometrical mean of the laser pulse length τ and the traverse time over the target by the sound speed.
Yin et al. Yin (2007) have found in their 3D simulation that for long pulse irradiation the pulse exhibits an epoch of burn-through (and relativistic transparency). This phenomenon is when the laser penetrates the target and eventually emerges from the rear end of the target. This corresponds precisely to the second period between t_1 and t_2 and in fact most of the acceleration takes place shortly after t_1. We now characterize the physical processes including these phenomena. Beyond time t_1, the plasma is relativistically transparent so that the laser can now interact with the (expanded) target plasma in its entirety. It can also now expand in three dimensions. For 3D isotropic expansion, it takes time Δt during which the normalized density reduces from γ to 1Yan (2009a) as:

$$\Delta t = \frac{Nd(\gamma^{1/3} - 1)}{\gamma C_s} \frac{1}{\sin((\pi/2\tau)t_1)}. \tag{6}$$

Now the time t_2, when the plasma becomes underdense, is given as $t_2 = \Delta t + t_1$.
We examine the physical situation at time t_1, when the laser pulse has penetrated the entire target with the relativistic transparency and we may regard that the laser begins to drive the entire plasma electrons from this already expanded target. An expression in a closed form for the ion energy gain between time t_1 and t_2 in the case of a laser pulse with a duration longer than the relativistic transparency (rt) time t_1 has been obtained expanding the idea in Eq. (4) as:

$$\varepsilon_{\mathrm{max},i,\mathrm{rt}} = (2\alpha + 1)\, Q\bar{\varepsilon}_0 \Big((1 + \omega_L(t_2 - t_1))^{1/2\alpha+1} - 1 \Big). \tag{7}$$

In Fig. 4 we plot the total energy gain in the case of carbon ions from this formula as a function of target thickness. Once again the optimum thickness, for which the ion gain is maximum, is sharply realized in the CAIL regime. Towards the TNSA regime the ion energy

decreases substantially. Thus theory has guided the experiments that (remakably) agree with the predictions Hegelich (2011).
It is noteworthy to consider how the photon pulse behaves right after the relativistic transparency time t_1. The group velocity of the laser pulse $v_{\rm gr} = c\sqrt{1-\omega_p^2/\omega_L^2}$ vanishes at $t = t_1$. At this moment the ponderomotive structure of photons is stationary, which pushes electrons as well as ions effectively forward. This is because the heavy and sluggish ions can respond easily to this stationary potential. As the laser penetrates further and the plasma density decreases below $n_{\rm cr}\cdot\gamma$, the group velocity begins to increase. In our model case Yan (2009a) of the laser temporal structure of $a_0 \propto \sin^2((\pi/2\tau)t)$, the group velocity increases as

$$v_{\rm gr}(t) \sim 2c\cot((\pi/2\tau)t_1)\sqrt{(\pi/2\tau)(t-t_1)}\,. \tag{8}$$

This means that the speed of the accelerating structure – made up of the electron layer driven by the laser ponderomotive force and the ion layer that is attached to the former by the electrostatic force – is picking up quickly from zero. This suggests that if we can slow down the photon group velocity, the rate of increase of the photon group velocity and thus the accelerating structure is reduced and, therefore, the adiabatic nature of acceleration becomes more pronounced. Such may be accomplished by increasing the density of the plasma behind the solid target by a further material. Nakamura et al. Nakamura (2010) have investigated near critical density acceleration, which is related to this point as seen in Eq.(8).

2.4.3 Radiation Pressure Acceleration (RPA)

Mono-energetic ion beams are one of the important requirements of ion beam therapy. The Coherent Acceleration of Ions (CAIL) by linearly polarized pulses can efficiently accelerate ions to higher energy by using nanometer targets. Recently, theoretical attention has focused on the use of circularly polarized (CP) laser pulses in the CAIL regime to accelerate high density ion bunches at the front surface of thin foils. For CP pulses, the ponderomotive force has no oscillating component as discussed; hence, electrons are steadily pushed forward, inducing a charge separation field which can accelerate ions. It is expected to provide a more adiabatic interaction so that mono-energetic ion beams may be realized, in this case in the regime called Radiation Pressure Acceleration (RPA). There is a regime of phase stable acceleration in the interaction of a CP laser with a thin foil in a certain parameter range, where the proton beam is synchronously accelerated and bunched like in a conventional radio frequency (RF) accelerator. This synchronous acceleration leads to the acceleration regime in which the position of ions is well tied with the accelerating structure made up of the laser ponderomotive potential and the electron layer. Therefore, ions may be trapped in this accelerating bucket, in which they may show a phase-stable behavior. That is, ions exhibit phase stable oscillations (synchrotron oscillations).
A simple model to elucidate the bunch formation in the phase stable acceleration has been considered Yan (2009a). We introduce the relative ion position $\zeta = (x_i - x_r)$ with the compressed electron layer $-l_s/2 \le \zeta \le l_s/2$, where $x_r = D + l_s/2$ represents the position for the center-of-mass reference particle. The force acting on a test ion is given by $F_i = q_i E_m (1-(x_i-D)/l_s)$. Thus, the equation of motion for the proton is

$$\frac{{\rm d}^2 x_i}{{\rm d}t^2} = \frac{Qe\,E_m}{m_i}\left(1-\frac{x_i-D}{l_s}\right). \tag{9}$$

Eq.(9) shows that the center of mass x_r moves with constant acceleration as

$$x_s = (1/2)(d/2)\omega_{pi}^2 t^2, \tag{10}$$

where $\omega_{pi}^2 = 4\pi e^2 Q n_0/m_i$, d and n_0 are the original foil thickness and electron density. The phase motion (ζ, t) around x_r is showing oscillatory motions:

$$\ddot{\zeta} = -\Omega^2\zeta, \;\; \Omega^2 = \frac{Qe\,4\pi e n_0 d}{m_i\, l_s}, \tag{11}$$

where Ω is called the frequency of the synchrotron oscillation motion in longitudinal direction Chao (1999). This means that the center of mass accelerates with a constant rate (in the nonrelativistic regime) as in Eq.(10), while the individual ions oscillate around the center trapped by the bucket.
The bucket velocity width may be determined from Eq.(11):

$$v_{i,\mathrm{buc}} = \zeta\Omega = \sqrt{\frac{m_e}{m_i}\, Q\, a_0}\, c\, N^{-1/4}\,. \tag{12}$$

This bucket size is close to (and slightly less than) the trapping velocity width from Eq.(3). As long as $N > \gamma$ (or $t \le t_1$), $v_{i,\mathrm{buc}} \le v_{i,\mathrm{tr}}$, while for $N < \gamma$ $(t > t_1)$ $v_{i,\mathrm{buc}} \ge v_{i,\mathrm{tr}}$ and some of the ions in the bucket begin to spill over.
The energy spread of trapped ions in the bucket of the accelerating structure with respect to the energy ε_r of the reference particle is

$$\Delta\varepsilon/\varepsilon_r = 2\,\zeta_0\,\Omega/\sqrt{2\,m_i\,\varepsilon_r}\,. \tag{13}$$

If we take $\zeta_0 = l_s/2$ and $\varepsilon_r = 400$ MeV, the energy spread will be less than 4 %, which agrees well with the simulation results.
In 1D simulations the plasma is kept cold and the target is pushed forward as a whole, so an ideal mono-energetic ion beam can be generated. A quasi-monoenergetic carbon ion beam with 17 % energy spread has been observed in recent experiments Henig (2009): $\Delta\varepsilon/\varepsilon_r \sim$ 17 % is about 3 times higher than the estimation by Eq.(13) because of the multi-dimensional effects. In real situations typically the laser intensity is not uniform, the transverse profile tends to bend the flat target, and foil electrons are heavily heated by the oblique incident laser, in spite of the CP pulse. If and when electrons become hot or the laser leaks through, the bucket begins to collapse and the energy spread drastically increases.

2.4.4 Improved acceleration schemes

When the electron dynamics is slow enough that ions evolve less suddenly, i. e. adiabatically Chao (1999), the final energy gain of electrons (and thus that of ions) may not be that of the instantaneous energy dictated by the expression of ε_0. For example, we have remarked a case with a circularly polarized pulse. In the latter, for example, the pulse should cause less electron energy gain than in the linearly polarized case. Therefore, the cloud of electrons cannot instantaneously shoot out of the foil, but rather leaves the target gradually. This renders a possibility that the electron energy is not only proportional to the field strength (as proportional to a_0), but also to the time during which electrons are accelerated by $v \times B$ if this is much longer than the laser period. When electrons substantially co-move with the laser pulse, this time can be proportional to a_0 or some fraction of it, leading to a proportionality greater than a_0 such as a_0^2. We anticipate more results to come in advancing the ion energy by laser acceleration spurred by the current theoretical understanding of the physics.

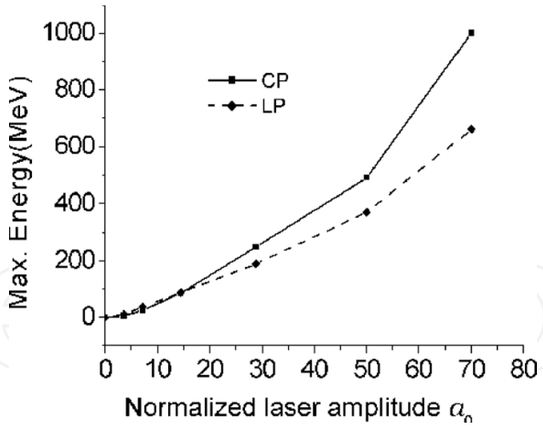

Fig. 5. Maximum proton energy versus a_0 obtained in 2D PIC simulations. In the modest a_0 regime ($15 \geq a_0 > 1$) the energy gains by LP and CP are not much different, while that by CP is much greater than by LP for large a_0 ($a_0 \geq 15$). The exponent to a_0 for CP seems to increase from less than 2 in $a_0 \leq 15$ towards 2 in $a_0 \geq 15$.

In PIC simulations, an a_0^2 scaling is observed in Rykovanov (2008) using circularly polarized (CP) laser pulses. However, this is only a 1D simulation and bending and boring effects are not considered. With 2D simulations, the scaling with the normalized vector potential a_0 is only $a_0^{1.1}$ in the linear polarized case (and the fit looks much better than Eq.(1), while for the circular case the maximum proton energy scales with $a_0^{1.6}$ at the lower intensity for $a_0 \leq 30$. It tends to be closer to an a_0^2 scaling for larger a_0 values (see Fig. 5), including the highly relativistic regime Esirkepov (2004). This tendency of having less energy (or a smaller exponent to a_0) in the 2D simulation than the one shown in the idealized 1D model, may be due to several reasons. One is the bending or bulging (the convex shaping as viewed from the rear surface, where ions are emitted) of the thin target by the impinging laser pulse. This causes the excess plasma electron heating by the obliquely incident laser electric fields and thus contributes to hot electrons that run away from the target leaving ions far behind, yielding non-adiabatic electrons and thus ion dynamics. Secondly, once the laser ponderomotive potential penetrates through the thin target, the till then slow motion of the ponderomotive potential now begins to pick up its speed, as the density of the plasma seen by the laser is less than the relativistic transparent density (in terms of the timing of the interaction corresponding to time t_1). Once the laser increases its group velocity in this less dense region, only electrons can keep up with photons, while ions are left behind. When this develops, we see that the nicely closed phase space circle is now skewed, eventually leading to a collapse of the bucket. (See details in Ref.Tajima (2009), there Figs. 18 and Fig. 19).

In order to further improve these situations, we envision to counteract the convex bulging by instituting a concave shape to the target. This little manipulation may improve the energy enhancement by a factor of a few Tajima (2005). A recent simulation demonstrates this Wang (2010). It should also help if we adopt a cone Kodama (2002) in front of the foil, which can collect the laser power to intensify the radiance of the laser. Wang et al. Wang (2011) have suggested a gas medium (in front of the thin foil) that leads to the enhanced laser intensity.
To further arrest the collapsing trapping bucket by the accelerating photons after they transmit through the thin target, we could let them slow down again by adding supplementary target material such as dense gas/clusters, a foam target or a mesh of carbon nanotubes behind the rear surface. Such would decrease the group velocity of the laser after it passes through the

thin solid foil and increase the interaction time between the laser pulse and the plasma and therefore the accelerating time for ions. With special target manufacturing techniques (e.g. concave as looked from the rear surface) or hemispheric targets, it may be possible to increase the power of a_0 in ion energy that is important as an outlook, because at present we need a much bigger laser if we want to reach the medical energy of 200 MeV/u. If these additional measures can enhance the ion acceleration time, it will be perhaps possible to reduce the necessary laser intensity and still reach the same energies, contributing to a less demanding laser power for the necessary energy regime.
Even if the necessary energies are reached, there are many additional requirements a therapy system needs to satisfy, as was discussed in Sec. 1. These are by no means easy tasks and pose challenges for us researchers. On the other hand, we do have a host of new ways to manipulate intense ion and laser beams by harnessing the relativistic dynamics of the laser and its plasma interaction Mourou (2006). For example, our ability to simultaneously generate an ion beam with coherent X-rays Tsakiris (2006) from the laser-thin target interaction can allow us to perform unprecedented accurate X-ray diagnosis such as phase contrast imaging Pfeiffer (2006). This would give us the additional ability of accurate imaging simultaneous with therapy. With the increasing ability to detect smaller tumors, the laser driven ion therapy method with the imaging guidance and with on-line dose verification techniques Bolton (2010); Kormoll (2011) may become a suitable clinical option for safe treatment of small tumors Murakami (2008).

3. Medical radioisotopes with high specific activity produced in photonuclear reactions

The laser-driven γ beams are spurring the possible clinical usage of a novel class of radioisotopes that are very useful for nuclear medicine but are not easy to obtain otherwise. These radioisotopes may be delivered to specific cells/DNA/proteins/peptides of the tumor with a specific vector drug, where cancer cells may be killed by their radioactivity. This method is not hampered by the beam scattering of ion therapy in Sec. 2, nor restricted by non-metastasis, which are the general limitations of EBRT.

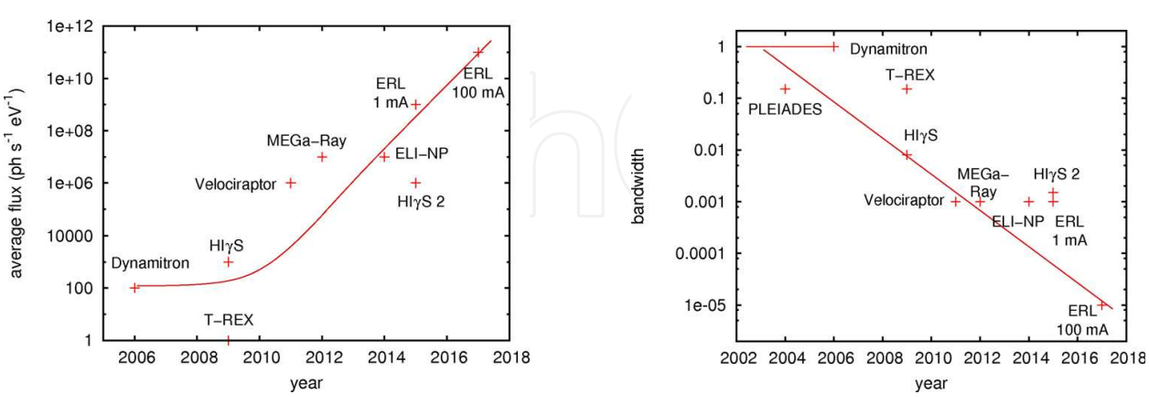

Fig. 6. Progress in flux of γ beams (left) and (right) progress in bandwidth $\Delta E_\gamma / E_\gamma$ of high-energy γ beams ($\approx$ 10 MeV) for different (existing and planned) γ beam facilities.

In a new development the intense, high repetition rate, diode pumped lasers in combination with intense, brilliant, relativistic electron beams allow to produce very intense, brilliant γ beams via Compton back-scattering. Thus in about 2 years from now the MEGa-ray project

at LLNL Barty (2010) will have γ beams, which have $10^{(4-6)}$ times higher flux than the best existing γ beams and it can be anticipated from ongoing developments that in 5-10 years even 10^4 times more intense γ beams will become available, which will allow to produce many new medical radioisotopes for diagnostics and therapy. This is illustrated in Fig. 6. The new γ beams will also have a much smaller band width $\Delta E_\gamma / E_\gamma$, allowing to address individual nuclear levels with strong population. Here, on the one hand, by (γ, γ') photoexcitation new nuclear isomers can be produced, which decay frequently by many conversion and Auger electrons, allowing for a short-range killing of tumor cells in the surrounding 10-200 μm range after they have been transported to the overexpressed acceptors of the cancer cells. But also by $(\gamma, xn + yp)$ photonuclear reactions many new medical radioisotopes can be produced. We will discuss in detail many new specific radioisotopes. As an example we here want to mention so-called "matched" pairs for diagnostics and therapy of the same chemical element. Here pairs like: ^{44}Sc/^{47}Sc, ^{61}Cu or ^{64}Cu/^{67}Cu, ^{86}Y/^{90}Y, ^{123}I or ^{124}I/^{131}I or ^{152}Tb/^{149}Tb or ^{161}Tb are of special interest, where one of the isotopes was so far difficult to produce by classical methods. Here the basic idea is to use bioconjugates Schiepers (2006), that show a high affinity and selectivity to bind to peptide receptors or antigens, that are overexpressed on certain cancer cells compared to normal cells. As shown in Fig. 7 the suitable radioisotope is placed into the chelator end of the bioconjugate. These therapies are called Peptide Receptor Radio Therapy (PRRT), when peptides are used as bioconjugates or radioimmunotherapy (RIT), when antibodies are used. This therapy allows to fight diseases, which are not localized or cancer types with multiple metastasis. Once the suitable radioisotopes have been produced the main task stays with radiochemistry and radiopharmaceutics to build the proper bioconjugates to reach the cancer cells in the optimum way. While we are pushing for the treatment of very small tumors in laser-driven ion therapy, with the new therapeutic medical radioisiotopes one is going for shorter range emitted radiation (α particles, low-energy electrons) only killing cancer cells and cancer stem cells in the immediate surrounding, where the bioconjugate was delivered.

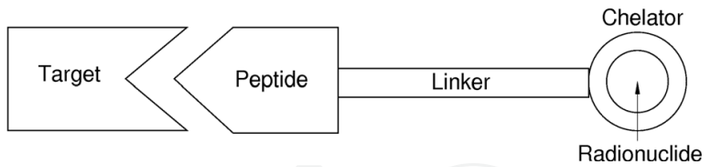

Fig. 7. Schematic picture explaining how a specific radionuclide can be transported to a specific peptide receptor.

3.1 Brilliant γ beams

In the next years γ beams, presently under construction, will become available with that much increased flux, that a good production of medical radioisotopes becomes possible. These γ beams are produced via Compton back-scattering of laser photons from a relativistic electron beam. photonuclear physics is the High-Intensity γ-ray Source (HIγS) at Duke University (USA). It uses the Compton back-scattering of photons, provided by a high-intensity Free-Electron Laser (FEL), in order to produce a brilliant γ beam. The γ intensity in the energy range between 1 MeV and 160 MeV amounts to $10^8 s^{-1}$ with a band width of about 5% Weller (2009). There are plans to upgrade the facility by using infrared laser light in a longitudinal enhancement cavity to increase the intensity to $2 * 10^{12} s^{-1}$ and the band width to about 0.1 - 0.2 % Wu (2011). Besides the storage ring approach an approach with a electron linac is persued. Here the project T-REX with a normal conduction S-band electron linac was

recently terminated Albert (2010; 2011). Here a new brilliant Mono-Energetic Gamma-ray (MEGa-ray) facility at Lawrence Livermore National Laboratory (USA) is based on a normal conducting 12 GHz electron linac and should yield already in the beginning of 2013 for γ energies between 0.5 and 4 MeV a γ intensity of $10^{13}s^{-1}$ with an energy band width of down to 10^{-3} and a brilliance of $10^{22}/[\mathrm{mm}^2\mathrm{mrad}^2\mathrm{s}\ 0.1\%\mathrm{BW}]$ Barty (2010). Using the same accelerator technology, at the upcoming Extreme Light Infrastructure - Nuclear Physics (ELI-NP) facility in Bucharest, a γ beam will become available until 2015, providing about the same γ intensity and band width in the energy range of 1-25 MeV ELINP (2010). Even more efficient interactions between electron bunches and laser pulses from diode pumped lasers are under investigation, which will improve the γ flux from the presently given value of $10^6/(\mathrm{eVs})$ by two orders of magnitude.

At present, great efforts are also invested all over the world to realize highly brilliant γ beams based on the Energy Recovery Linac (ERL) technology. The Energy Recovery Linac (ERL) requires a new type of superconducting electron accelerator that provides a highly brilliant, high-intensity electron beam. The main components of an ERL are an electron injector, a superconducting linac, and an energy recovery loop. After injection from a highly brilliant electron source, the electrons are accelerated by the time-varying radio-frequency field of the superconducting linac. The electron bunches are transported once through a recirculation loop and are re-injected into the linac during the decelerating RF phase of the superconducting cavities. So the beam dump has to take the electron bunches only with low energy, while the main part of the electron energy is recycled. At ERLs highly brilliant γ beams can be created by Compton back-scattering of photons with high energy (0.1-100 MeV), again recirculating the photons in a high finesse cavity with MW power or using ring-down cavities to overcome the small Compton cross section. ERL technology is pioneered at Cornell University (together with Thomas Jefferson National Laboratory) Bilderback (2010a;b); Liepe (2010), where an ERL is presently under construction for a 5 GeV, 100 mA electron beam. $> 10^{16}s^{-1}$ in an energy range of 0.5 - 25 MeV. Such a facility would provide a brilliant pulsed γ beam with a narrow band width much smaller than 10^{-3} and very high flux of $(10^{10} - 10^{11})/(\mathrm{eVs})$. Since due to thermal Doppler-boadening the nuclear levels have typical widths of a few eV, good yields for medical isotopes are expected. For the new γ beams with better band width and small opening angle, we may use arrays of refractory γ lenses Schroer (2005); Vaughau (2011). In this way we could focus the γ beams to very small spot size (10 nm) for the first time and it becomes feasible to always use enriched targets for medical radioisotopes with high specific activity.

3.2 Presently used nuclear reactions to produce medical radioisotopes

Today the most frequently employed nuclear reactions for the production of medical radioisotopes are:

1. **Neutron capture** Neutron capture (n,γ) reactions transmute a stable isotope into a radioactive isotope of the same element. High specific activities are obtained, if the (n,γ) cross section is high and the target is irradiated with a high neutron flux. Neutrons most useful for (n,γ) reactions have energies from meV to keV (thermal and epithermal neutrons) and are provided in the irradiation positions of high flux reactors at flux densities of 10^{14} n/(cm^{2}s) up to few 10^{15} n/(cm^{2}s). If the neutron capture cross section is sufficiently high (e.g. 2100 barn for ^{176}Lu(n,γ)^{177}Lu), then a good fraction of the target atoms can be transmuted to the desired product isotopes, resulting in a product of high specific activity.
2. **Nuclear fission** Fission is another process used for isotope production in nuclear reactors. Radiochemical separation leads to radioisotopes of "non-carrier-added" quality, with

specific activity close to the theoretical maximum. Fission is the dominant production route for the generator isotopes ^{99}Mo and ^{90}Sr, for the β^- emitting therapy isotope ^{131}I and for the SPECT isotope ^{133}Xe.

3. **Charged particle reactions with p, d or α ions** Imaging for diagnostic purposes requires either β^+ emitters for PET (mainly ^{18}F, ^{11}C, ^{13}N, ^{15}O, ^{124}I, or ^{64}Cu), or isotopes emitting gamma-rays with suitable energy for SPECT (about 70 to 300 keV), if possible without $\beta^{+/-}$ emission to minimize the dose to the patient. Thus electron capture decay is preferred for such applications, e.g.: ^{67}Ga, ^{111}In, ^{123}I, ^{201}Tl. Usually these neutron-deficient isotopes cannot be produced by neutron capture on a stable isotope (exception ^{64}Cu). Instead, they are mainly produced by charged-particle induced reactions such as (p,n), (p,2n),... High specific activities of the final product are achievable, if the product differs in chemical properties from the target (i.e. different Z) and can be chemically separated from the remaining bulk of target material. Thus Z must be changed in the nuclear reaction, e.g. in (p,n), (p,2n), (p,α) reactions. The energies of the charged particle beams for such reactions are usually in the range of 10 to 30 MeV and can be supplied with high currents (0.1 to 1 mA) by small cyclotrons.
4. **Generators** Another important technique is the use of generators, where short-lived radionuclides are extracted "on-tap" from longer-lived mother nuclides. Here the primary radioisotope (that was produced in the nuclear reaction) has a longer half-life than the final radioisotope (that is populated by decay of the primary radioisotope and is used in the medical application). The primary radioisotope is loaded onto the generator and stays there chemically fixed. The final radioisotope will grow in and can be repetitively eluted and used.
5. **Photonuclear reactions** The inverse process to (n,γ), namely (γ,n), also allows producing neutron deficient isotopes, but conventional γ ray sources do not provide sufficient flux density for efficient production of radioisotopes with high total activity and high specific activity. Therefore, this process played no role until now.

4. Specific radioisotopes produced in photonuclear reactions

We now discuss in detail the different γ-induced reactions and specific radioisotopes that can be produced by photonuclear reactions, that are enabled by the aforementioned breakthroughs of brilliant γ beam technology. In Tables 1 and 2 we show estimates of the achievable specific activities for thin targets for a γ flux of 10^{14} per s, corresponding to a flux density of 10^{18} $\gamma/(\mathrm{cm}^2\ \mathrm{s})$ for a beam cross-section of $(0.1\mathrm{mm})^2$. With a bandwidth of 10^{-3}, this results at 10 MeV in a spectral flux density of 10^{14} $\gamma/(\mathrm{cm}^2\ \mathrm{s\ eV})$. With γ lenses the beam cross section could be improved by 10^4 and a better bandwidth is expected. We compare these to thin-target yields obtained by thermal neutron capture at a typical flux density of 10^{14} $\mathrm{n}/(\mathrm{cm}^2$ s) in high flux reactors. Note that alike for the potential beam parameters of γ beam facilities, there is also a wide range of flux densities available at the irradiation positions of high flux reactors. Some positions provide flux densities of several 10^{12} to 10^{13} $\mathrm{n}/(\mathrm{cm}^2$ s), while few special reactors have positions that even exceed 10^{15} $\mathrm{n}/(\mathrm{cm}^2$ s), namely SM3 in Dimitrovgrad Karelin (1997), HFIR in Oak Ridge Knapp (2005) and the ILL's high-flux reactor in Grenoble.
Since hitherto no γ beams with sufficiently small bandwidth were available to exploit resonant excitation, there are obviously no such measured cross-sections. Presently, we can only estimate a lower bound using the averaged cross-sections measured at bremsstrahlung facilities Carroll (1991;a;b); data (2010); Neumann (1991). For cases where no measured cross-sections are available, we interpolate experimental cross-sections of the same reaction

channel on nearby elements, taking into account the energy above the reaction threshold. We have submitted a proposal to the HIγS facility to measure the expected strong resonant gateway states for radioisotope production, which frequently can be predicted from known neighboring nuclei.
Even when using conservative assumptions, the estimated specific activities are promising for specific isotopes.
The total radioisotope activity achievable in a nuclear reactor can be relatively high since, thick (several cm) and large (several cm^2) targets can be used if the cross-sections are not too high (leading to self absorption and local flux depression). Multiple irradiation positions allow producing various radioisotopes with activities of many TBq.
For the γ beam we estimate the total activities by integrating to one interaction length, i.e., where the initial γ-beam intensity has dropped to $1/e = 37$ % of its intensity. Higher total activities can be achieved with thicker targets at the expense of lower specific activity and vice versa. The total interaction cross-section is usually dominated by the atomic processes of Compton effect and pair creation, but not for γ beams with very small bandwidth. We conservatively consider any γ ray as lost after interaction. In reality, part of the Compton scattering goes forward under small angles and the γ rays that have lost little energy can still induce photonuclear reactions. The usable target thickness ranges from 20 g/cm^2 for heavy elements to 40 g/cm^2 for light elements, i.e., in total only few mg target material are exposed to the small area of the γ beam. With non-resonant reactions of the order of 0.1 TBq activity can be produced per day, corresponding to tens (for β^- therapy isotopes) to thousands (for imaging isotopes and therapy with alpha emitters) of patient doses.

4.0.1 Isomers of stable isotopes via (γ, γ') reactions

For various applications in nuclear medicine longer-lived nuclear isomers that decay by emission of gamma rays and/or conversion electrons to the respective ground state are of

Isotope	Isomer			I_{is}/I_{gs}	Ground state		$\sigma \cdot \Gamma$		Sep.	Act.	R_γ	Sp.Ac.	$R_\gamma/$
	Exc. energy keV	Spin & parity	$T_{1/2}$ d		Spin & parity	Nat. abun. %	at 4 MeV eV·b	at 6 MeV eV·b	Act. γ	1/d GBq	fraction of max.	high flux reactor GBq/mg	$R_{(n,\gamma)}$
^{87}Sr	389	$1/2^-$	0.12	3.5	$9/2^+$	7	3.9	8.7	10	110	$2{\cdot}10^{-5}$	0.57	18
^{115}In	336	$1/2^-$	0.19		$9/2^+$	95.7	18	67	58	603	$3{\cdot}10^{-4}$		
^{117}Sn	315	$11/2^-$	13.8	0.04	$1/2^+$	7.68	3.2	8.8	7.5	0.6	0.0025	0.003	2400
^{123}Te	248	$11/2^-$	119	0.13	$1/2^+$	0.89	42	68	55	0.6	0.17	0.2	280
^{125}Te	145	$11/2^-$	57.4	0.17	$1/2^+$	7.07	70				0.08	0.48	
^{129}Xe	236	$11/2^-$	8.9	0.10	$1/2^+$	26.4						0.2	
^{131}Xe	164	$11/2^-$	11.8	0.10	$3/2^+$	21.2						0.2	
^{135}Ba	268	$11/2^-$	1.2	0.08	$3/2^+$	6.59	13	60	44	33	$1.5{\cdot}10^{-3}$	0.045	1000
^{176}Lu	123	1^-	0.15	2.0	7^-	2.59	140	350	2.0	1800	$1.2{\cdot}10^{-3}$	5.5	36
^{195}Pt	259	$13/2^+$	4.02	0.09	$1/2^-$	33.8	30	140	72	17	0.012	0.019	3800

Table 1. Longer-lived nuclear isomers produced in (γ, γ') reactions. The relative population of the respective isomer in thermal neutron capture on A-1 target isotopes is given as I_{is}/I_{gs} where known experimentally. Experimental integrated cross sections for population of the isomer by (γ, γ') reactions at 4 MeV and 6 MeV were taken from Carroll (1991;a). The fraction of the maximum specific activity R_γ produced in (γ, γ') reactions is put in relation to the one obtained with (n,γ) reactions $R_{(n,\gamma)}$ at a thermal neutron flux of 10^{14} n/(cm^2 s) in the last column.

interest, if they can be produced with high specific activity. Table 1 shows a selection of such isomers.

Most usual production methods, e.g., via (n,γ) reactions, result in relatively low specific activity, since the dominant part of the production proceeds directly to the nuclear ground state that has a nuclear spin closer to that of the A-1 target isotope. However, the fact that all these isomers are actually populated via thermal neutron capture reactions on low-spin A-1 target isotopes proofs that pathways populating the high-spin isomers from higher-lying, low-spin compound nucleus resonance levels of lower spins must exist. In Ref. Lendoux (2006) the population of high-spin isomers relative to the ground state was studied for resonances in (n,γ) reactions. An energy dependence of the isomeric ratio was observed. One may expect that this energy dependence would become even more pronounced if the reactions were excited with a primary beam of smaller bandwidth that populates more selectively states which decay mainly to the isomeric level of interest.

Also photoexcitation (γ, γ') experiments with bremsstrahlung beams were performed on a series of stable targets and showed strong population of isomeric levels Carroll (1991;b); Neumann (1991). The observed energy dependence of the isomer activation yields indicates that few gateway states are responsible for efficiently populating the isomers.

Moreover, photoexcitation with small-bandwidth γ rays allows the selective excitation of individual levels or groups of levels that decay preferentially to the nuclear isomer, thus enhancing the specific activity of the isomer. Only in few cases the energies of such (groups of) levels are already known. Note that relatively low gamma ray energies may be sufficient for such a pumping to isomeric states. In ^{125}Te a $7/2^+$ state at only 402 keV excitation energy can serve as gateway state for pumping from the $1/2^+$ ground state to the $11/2^-$ isomer at 145 keV NuDAT (n.d.).

We will estimate the achievable specific activity at the example of ^{115}In, for which the required transition energies, branching ratios and transition strengths are already experimentally known, even if this isomer has presently no application in nuclear medicine.

Experimental data on isomer population by (γ, γ') reactions have so far been obtained with bremsstrahlung spectra of large bandwidth. The integrated cross-sections at γ energies of 4 and 6 MeV, respectively, are of the order of 10 to 100 b·eV.

Many potential gateway states that could serve for pumping nuclei from their ground state to isomeric levels are expected to exist, but they still need to be identified by dedicated high resolution measurements from excitation energies of few hundred keV up to close to the particle separation energy. These measurements have to be performed with the new γ beams for each of the isotopes for variable energy windows, in order to determine the best excitation-deexcitation path to the isomer. Presently existing γ-ray beam facilities only marginally provide sufficiently monochromatic γ-ray beams to search for suitable resonance regions. A systematic investigation will require Compton backscattering facilities such as MEGa-ray (LLNL) or ELI-NP.

Selecting γ ray energies providing strong pumping to the isomeric state will improve the achievable specific activity correspondingly. Even multiple excitations of the path to the isomer are possible. Due to the missing energy match, no significant back-pumping from the isomer to the ground state will occur.

maximum specific natural abundance and assume that finally will result in a total conversion of the ground than presently

Two examples of long-lived isomers with important medical applications are discussed in the following:

1. ^{195m}Pt: Platinum compounds such as cisplatin or carboplatin are known to be cytotoxic and are frequently used for chemotherapy of tumors. Labeling these compounds with platinum radiotracers allows for in-vivo pharmacokinetic studies and tumor imaging, e.g., to monitor the patient-specific uptake and optimize the dosing individually Dowell (2000). Failure to demonstrate the tumor uptake of the chemotherapy agent by nuclear imaging helps to exclude those "non-responding" patients from unnecessary chemotherapy treatment. ^{195m}Pt has 4 days half-life and emits a 99 keV gamma ray that can be used for imaging by SPECT or gamma cameras. ^{195m}Pt emits also low-energy conversion and Auger electrons. Hence, when used in higher activities, it could be suitable for a combined chemo- and radionuclide therapy. Unfortunately, ^{195m}Pt is destroyed by (n,γ) reactions with a very high cross section of 13000 barn. Therefore the specific activity achievable by neutron capture on ^{194}Pt is seriously limited.
2. ^{117m}Sn: Also, ^{117m}Sn emits low-energy conversion and Auger electrons, making it promising for radionuclide therapy. In addition it emits a 159 keV gamma ray for imaging. It has been shown that ^{117m}Sn can be used for pain palliation in bone metastases of various cancers. Due to its soft electron energy spectrum, it has less side effects on the bone marrow than other radioisotopes with more penetrating radiation Bishayee (2000).

These two isomers appear at present most interesting for nuclear medicine applications.
The specific activity and total production per day could be significantly improved with still to be found better gateway states. A detailed search for suitable gateway states at an upcoming γ-beam facility with small bandwidth is underway.

4.1 Radioisotopes via the (γ,n) reaction

When excited well beyond the neutron binding energy, a nucleus readily loses a neutron. Competing reactions such as deexcitation by gamma ray emission are far less probable.

1. ^{99}Mo/^{99m}Tc: The presently most used radioisotope for nuclear medicine studies is ^{99m}Tc. Its 140 keV γ ray is ideal for SPECT imaging. With a relatively short half-life of 6 h and the quasi-absence of beta particles, the radiation dose to the patient is sifficiently low. ^{99m}Tc is conveniently eluted in non-carrier-added quality from simple and reliable ^{99}Mo ($T_{1/2} =$ 66 h) generators that can be used for about one week. Various technetium compounds have been developed for a multitude of nuclear medicine applications Schiepers (2006). The combination of these advantages explains why ^{99m}Tc is used in about 80% of all nuclear medicine studies. Until recently five nuclear reactors were used to produce about 95 % of the world needs of ^{99}Mo by neutron-induced fission of highly enriched ^{235}U targets. Recently the two reactors that used to produce the majority of the ^{99}Mo supply had extended shutdowns, leading to a serious ^{99}Mo/^{99m}Tc supply crisis Lewis (2009); Raloff (2009). A facility providing $10^{15}\gamma$/s could produce via ^{100}Mo(γ,n) reactions several TBq per week. Since the present request is 3000TBq per week, many such facilities would be required to assure the worldwide ^{99}Mo supply.

   This example demonstrates that the new production method by γ beams is not intended to compete with large-scale production of established isotopes. The advantage of γ beams for radioisotope production lies clearly in the very high specific activity that can be achieved for radioisotopes or isomers that are very promising for nuclear medicine, but that are presently not available in the required quality or quantity.
2. ^{225}Ra/^{225}Ac: Alpha emitters are very promising for therapeutic applications, since the emitted alphas deposit their energy very locally (typical range of one to few cancer

Product isotope	$T_{1/2}$ d	Target isotope	Rct.	E_γ MeV	σ b	Spec. act. γ beam GBq/mg	Activity per day GBq	R_γ fraction of max.	Spec. act. HFR GBq/mg	$R_\gamma / R_{(n,\gamma)}$
^{47}Ca	4.5	^{48}Ca	(γ,n)	19	0.09	1100	400	0.05	0.9	1200
^{64}Cu	0.5	^{65}Cu	(γ,n)	17	0.09	830	1150	0.006	4	200
^{99}Mo	2.8	^{100}Mo	(γ,n)	14	0.16	960	350	0.06	0.08*	12000
^{103}Pd	17	^{104}Pd	(γ,n)	17	*0.05*	290	16	0.1	1.8	160
^{165}Er	0.4	^{166}Er	(γ,n)	13	0.3	1100	1100	0.016	4.7	230
^{169}Er	6.9	^{170}Er	(γ,n)	12	*0.3*	$\approx$ 800	130	$\approx$ 0.2	0.8	1000
13	*0.3*	$\approx$ 200	30	$\approx$ 0.5	170					
^{186}Re	3.7	^{187}Re	(γ,n)	15	0.6	$\approx$ 1400	320	$\approx$ 0.2	35	40
^{225}Ra	14.8	^{226}Ra	(γ,n)	12	*0.2*	$\approx$ 300	30	$\approx$ 0.2		
^{47}Sc	3.4	^{48}Ti	(γ,p)	19	*0.02*	250	100	0.009		
^{67}Cu	2.6	^{68}Zn	(γ,p)	19	*0.03*	260	115	0.01		
^{44}Ti	60 y	^{46}Ti	(γ,2n)	27	*0.01*	$\approx$ 0.5	0.008	$\approx$ 0.1		
22	0.02	$\approx$ 25	0.7	$\approx$ 0.1						
^{84}Sr	(γ,2n)	25	*0.02*	140	5.6	0.06				
^{224}Ra	3.7	^{226}Ra	(γ,2n)	16	*0.1*	$\approx$ 50	10	$\approx$ 0.01		

Table 2. Estimated production rates of radioisotopes produced in (γ,n), (γ,p) or (γ,2n) reactions. Experimental cross sections were taken from data (2010), estimated cross sections are marked in italics. The fraction of the maximum specific activity produced in (γ,x) reactions R_γ, is put in relation to that obtained with (n,γ) reactions $R_{(n,\gamma)}$ at a thermal neutron flux of 10^{14} n/(cm^2 s) in the last column. *: For comparison we show the values for ^{99}Mo produced by ^{98}Mo(n,γ). However, usually ^{99}Mo is produced by fission with much better specific activity.

cell diameters) with high linear energy transfer (LET) and, hence, high probability for irreparable double strand breaks. An alpha emitter coupled to a cancer cell specific bioconjugate can be used for targeted alpha therapy to treat disseminated cancer types (leukemia), micro-metastases of various cancers or to destroy chemo- and radiation-resistant cancer cells (e.g., glioblastoma). One promising alpha emitter is ^{225}Ac ($T_{1/2} = 10$ days) that decays by a series of four alpha decays and two beta decays to ^{209}Bi.

3. ^{169}Er: ^{169}Er decays with 9.4 days half-life by low-energy beta emission (100 keV average beta energy). These betas have a range of 100 to 200 μm in biological tissue, corresponding to few cell diameters. The short beta range makes this isotope very interesting for targeted radiotherapy Uusijaervi (2006).
4. ^{165}Er: ^{165}Er is one example for an isotope that decays mainly by low-energy Auger electrons. Their range is shorter than one cell diameter. Hence, these Auger emitters have to enter the cell and approach the cell's nucleus to damage the DNA and destroy a cell. Coupled to a bioconjugate that is selectively internalized into cancer cells it can enhance the ratio for dose equivalent delivered to the tumor cell with respect to normal cells. This should result in an improved tumor treatment with less side effects.
5. ^{47}Sc: ^{47}Sc is a promising low-energy beta emitter for targeted radiotherapy. Scandium is the lightest rare earth element. Most established labeling procedures for valence III metals (Y, Lu,...) can be applied directly for Sc. Its 159 keV gamma line allows imaging of ^{47}Sc distribution by SPECT or gamma cameras. Alternatively, the β^+ emitting scandium isotope ^{44}Sc can be used for PET imaging as a "matched pair". Carrier-free ^{47}Sc can be produced by ^{50}Ti(p,α) or ^{47}Ti(n_{fast},p) reactions followed by chemical separation. The

alternative production via ^{46}Ca(n,γ)^{47}Ca$\rightarrow^{47}$Sc is uneconomic due to the extremely low natural abundance of ^{46}Ca.

6. ^{64}Cu: ^{64}Cu is a relatively long-lived β^+ emitter ($T_{1/2} = 12.7$ h) with various applications in nuclear medicine Anderson (2009). ^{64}Cu-ATSM is a way to measure hypoxia of tumors. Hypoxia is an important effect influencing the resistance of tumor cells against chemo- or radiation therapy. ^{64}Cu can also act itself as therapeutic isotope due to its emission of β^- (191 keV mean energy) and low-energy Auger electrons.
7. ^{186}Re: ^{186}Re is a radioisotope suitable for bone pain palliation, radiosynovectomy and targeted radionuclide therapy. Rhenium is chemically very similar to its homologue technetium, thus known compounds that have been developed for imaging with ^{99m}Tc can also be labeled with ^{186}Re and used for therapy. ^{186}Re is currently either produced by neutron capture on ^{185}Re, resulting in limited specific activity, or by ^{186}W(p,n) reactions followed by chemical Re/W separation. Enriched ^{187}Re targets should be used to minimize contamination of the product with long-lived ^{184,184m}Re by ^{185}Re(γ,n) reactions.

4.2 Radioisotopes via the (γ,p) reaction

Even when excited beyond the proton binding energy, a nucleus does not necessarily lose a proton. The latter is bound by the Coulomb barrier, leading to a suppression of the proton loss channel. Only for an excitation well beyond the proton binding energy, the proton gains enough kinetic energy for tunneling efficiently through the Coulomb barrier. However, such excitation energies are usually also above the neutron binding energy or even the two-neutron binding energy. Hence neutron emission competes with proton emission and the cross sections for (γ,p) reactions may be one order of magnitude lower than the competing channels. Thus, the achievable specific activity (specific activity with respect to the target mass) is limited for (γ,p) reactions. However, the product isotope differs chemically from the target since it has one proton less ($Z_{\text{product}} = Z_{\text{target}} - 1$). After irradiation, a chemical separation of the product isotope from the target can be performed, ultimately resulting in a high specific activity that is only compromised by competing reactions leading to other isotopes of the product element (such as (γ,np), (γ,2n)EC/β^+, etc.) or product burn-up by (γ,n).

1. ^{47}Sc: Besides the ^{48}Ca(γ,n)^{47}Ca$\rightarrow^{47}$Sc reaction, ^{47}Sc can also be produced via the ^{48}Ti(γ,p) ^{47}Sc reaction. The established Sc/Ti separation schemes can be employed for the chemical processing. Compared to the ^{47}Ti(n,p) way here the direct production of disturbing long-lived ^{46}Sc (via ^{46}Ti(n,p) or ^{47}Ti(γ,p), respectively) can be limited more easily, since ^{48}Ti is the most abundant titanium isotope and can be enriched more easily to high abundance. However, the irradiation times have to be kept relatively short to prevent excessive formation of ^{46}Sc impurity by ^{47}Sc(γ,n) reactions.
2. ^{67}Cu: ^{67}Cu is also a promising beta-emitter for targeted radiotherapy. Alike ^{47}Sc it has a sufficiently long half-life for accumulation in the tumor cells when bound to antibodies and its 185 keV gamma ray allows imaging with SPECT or gamma cameras. Together with the PET imaging isotopes ^{61}Cu or ^{64}Cu, it forms a "matched pair". The usual production routes ^{68}Zn(p,2p), ^{70}Zn(p,α), or ^{64}Ni(α,p) are all characterized by low yields. The former requires energetic protons ($\gg$ 30 MeV from larger cyclotrons) and the latter two methods use expensive enriched targets with low natural abundances.
3. Isotopes with higher Z: In principle, also heavier β^- emitters used for radionuclide therapy such as ^{131}I, ^{161}Tb or ^{177}Lu could be produced by (γ,p) reactions (on ^{132}Xe, ^{162}Dy

or ^{178}Hf targets respectively). However, for higher Z the increasing Coulomb barrier leads to small production cross sections.

thyroid problems. produced by thermal neutron-induced fission of enriched ^{235}U targets. be produced via ^{132}Xe(γ,p) reactions. particularly useful thin xenon gas targets. The handling of highly active stream is stongly reduced. Strongly enriched ^{132}Xe can be obtained **?**. gas target is straightforward, e.g. xenon gas cell with sterile water established t ^{124}Xe(p,2n) the thermal stress of the due to the Moreover the full recovery essentiel far cheaper than ^{124}Xe.

short-lived ^{225}Fr that ^{225}Ra. This reaction can be used simultaneously to production.

4.2.1 Radioisotopes via the (γ,2n) reaction

1. ^{44}Sc: ^{44}Sc is a promising metallic PET tracer that emits a 1157 keV gamma-ray quasi-simultaneously with the positron. With a suitable detection system (Compton telescope plus PET camera), a triple coincidence (gamma rays of 511 keV, 511 keV, and 1157 keV) can be detected Grignon (2007). Hence, for each triple-event the point of emission is derived instead of the usual line-of-response, leading to improved position resolution at reduced dose to the patient. Moreover, ^{44}Sc forms a "matched pair" with ^{47}Sc, a therapy isotope discussed above. ^{44}Sc can be obtained from ^{44}Ti/^{44}Sc generators where the parent isotope ^{44}Ti is very long-lived ($T_{1/2}$ = 60 years). Despite the very favorable properties of ^{44}Sc, this isotope is not yet used in clinical routine, since the generator isotope ^{44}Ti is difficult to produce and therefore prohibitively expensive until now.

   conveniently eluted on-site from generators and used for various **?**. The great interest in ^{68}Ga rapidly rising demand for presently produced by ^{69}Ga(p,2n) reactions that alternative production path.

   β^+ emitter is continuously ^{82}Sr/^{82}Rb of heart and brain. imaging with ^{99m}Tc **?**. PET imaging and the present ^{99}Mo/^{99m}Tc supply ^{82}Sr/^{82}Rb generators. produced in ^{85}Rb(p,4n)^{82}Sr reactions. few large cyclotrons or linear accelerators exist world-wide that ($\geq$ 60 MeV) for efficient ^{85}Rb(p,4n)^{82}Sr reaction. by photonuclear ^{84}Sr(γ,2n)^{82}Sr high specific activities are reached not to compromise sufficiently high per day
2. ^{224}Ra/^{212}Pb/^{212}Bi: Via ^{226}Ra(γ,2n) reactions the isotope ^{224}Ra ($T_{1/2}$ = 3.66 d) from the thorium chain can be obtained, where the noble gas ^{220}Rn isotope can be extracted easily. The α emitter ^{212}Bi ($T_{1/2}$ = 60 min) in this decay chain or its mother isotope ^{212}Pb are also considered for targeted alpha therapy, e.g., for malignant melanoma metastases Hassfjell (2001); Mia (2005).

With the new γ beam facilities like ELI-NP or MEGa-ray LLNL we will search for optimum gateway states for all these new medical radioisotopes, making the production cross section much more reliable.

5. Conclusion

The advance of intense laser technology Mourou (2006) is changing the reach of laser-driven approaches of radiotherapy, both in the EBRT and in the endoradiation therapy, taking advantage of the new brilliant γ beams. In terms of EBRT, the laser-driven ion beam therapy awaits the rapid progress in the understanding of laser ion acceleration, both theoretically and experimentally. Theoretically, the recent year's research now directs us where the "sweat spots" in reaching 100-200 MeV ion/nucleon with a 100-200 TW laser. Experimentally, so

far often with less than 100 TW lasers we now see convergence of experimental results with theory of more efficient regimes such as CAIL/RPA. Thus when near future experiments are expected to embark on PW lasers, these experiments should reveal not only sufficiently high ion energies mentioned above, but also the parameters and configurational dependencies for the "sweat spots". We then can optimize the overall best spots of operation. In going to smaller tumors ($\leq$ cm regime), it is important to develop the image guided irradiation with pencil beams (e.g. Ref. Sutherland (2010)), the online dosimetry with sufficiently agile novel methods of detection such as prompt γ detection from the proton beam collisions with tissue nuclei Kormoll (2011). Such guidance, irradiation, and dose confirmation can make up an active feedback dose delivery by a radio-oconcologist Murakami (2008) first time ever. This approach should lead to more accurate dose control over small tumors. This concept matches with the desire of the radiooncologist Molls (2009) to treat early small tumors, but also opens the avenue through which the laser-driven particle therapy can find niches when this method is ill-suited for larger tumors. The fledgling irradiation demonstrations by laser-driven proton beams on in vivo cells have shown, so far, the radiological effectiveness not far different from conventional accelerators Kraft (2010); Yogo (2009).
For the production of medical radioisotopes for nuclear medicine, we develop generalized nuclear models of doorway states for optimum production and start testing them with present γ beams of improved band width, compared to formerly published broad band width measurements. Even in the old measurements very strong variations of the production cross sections between different isotopes had been observed Carroll (1991), pointing to a nonstatistical cross section behavior. Thus we expect to find with MEGa-ray (LLNL) and ELI-NP in the next 3-5 years improved resonant cross sections, making this alternative way of medical radioisotope production more favorable and economical. The resonantly enhanced strong cross sections, with their narrow width compete much more favorably with the always present atomic cross sections. With these new intense, brilliant γ beams and γ optics the area of *nuclear photonics* starts, where nuclear collective doorway states are not only interesting from the perspective of nuclear modelling, but reach applicational importance like in nuclear medicine.

6. Acknowledgements

We thank M. Gross, C. Barty, P. Thirolf, V. Zamfir, A. Henig, D. Kiefer, D. Jung, R. Hörlein, J. Schreiber, M. Hegelich, S. Steinke, M. Schnürer, T. Sokollik, P. V. Nickles, W. Sandner, J. Meyer-ter-Vehn, Y. Kishimoto, Y. Fukuda, S. Kawanishi, S. Bulanov, T. Esirkepov, K. Kondo, M. Molls, F. Nüsslin, C. Ma, P. Bolton, F. Pfeiffer, M. Murakami, M. Abe, J. E. Chen, Y. R. Lu, Z. Y. Guo, Z. M. Sheng and F. Krausz for fruitful discussion and help.
This work was partly supported by Deutsche Forschungsgemeinschaft (DFG) through Transregio SFB TR18 and the DFG Cluster of Excellence Munich-Centre for Advanced Photonics (MAP).

7. References

M. Abe, Proc. Jpn. Acad.,Ser. B 83(6):151-162 (2007);
F. Albert et al., Opt. Lett. 35, 354 (2010).
F. Albert et al., Phys. Rev. STAB 13, 070704 (2011).
M. Allen *et al.*, Phys. Plasmas 10, 3283 (2003).
C.J. Anderson and R. Ferdani, Cancer Biother. Radioph. 24, 379 (2009).
A. Andreev *et al.*, Phys. Rev. Lett. 101, 155002 (2008).

M. Ashour-Abdalla etal., Phys. Rev. A23, 1906 (1981).
C. Barty, *Development of MEGa-Ray technology at LLNL*; http:/www.eli-np.ro/executive committee-meeting-april12-13.php (2010).
G.J. Beyer, Hyp. Interactions 129, 529 (2000).
D.H. Bilderback et al., New Jour. of Phys. 12, 035011 (2010).
D.H. Bilderback et al., Synch. Rad. News 6, 32 (2010).
A. Bishayee et al., J. Nucl. Med. 41, 2043 (2000).
P.R. Bolton et al., NIM A 620, 71 (2010).
C.A. Boswell and M.W. Brechbiel, Nucl. Med. Biology 34, 757 (2007).
W.J. Brown et al., Phys. Rev. ST AB 7, 060702 (2004).
F. Buchegger et al., Eur. J. Nucl. Med. 33, 1352 (2006).
S. V. Bulanov and V. S. Khoroskhov, Plas. Phys. Report 28, 453 (2002).
S. V. Bulanov *et al.*,C. R. Physique , 10, 216 (2009).
J.J. Carroll et al., Phys. Rev. C 43, 1238 (1991).
J.J. Carroll et al., Phys. Rev. C 43, 897 (1991).
J.J. Carroll et al., Phys. Rev. C 48, 2238 (1993).
T. Ceccotti *et al.*, Phys. Rev. Lett. 99, 185002 (2007).
A. Chao and M. Tigner, "Handbook of Accelerator Physics and Engineering" (World Scientific, Singapore, 1999).
E. Clarke, *et al.*, Phys. Rev. Lett. 84, 670 (2000).
G.J.R. Cook, *Clinical Nuclear Medicine*, Hodder Arnold Publisher, London (2006).
http://www.nndc.bnl.gov/exfor/(2010)
J.A. Dowell et al., Adv. Drug Deliv. Rev. 41, 111 (2000).
http:/www.eli-np.ro/
E. Esarey and M. Piloff, Phys. Plasmas 2, 1432 (1995).
T. Esirkepov *et al.*, Phys. Rev. Lett. 92 (17), 175003 (2004).
T. Esirkepov *et al.*, Phys. Rev. Lett. 96, 105001 (2006).
J. Fuchs *et al.*, Nature Physics 2, 48 (2006), and refs. therein.
Y. Fukuda *et al.*, Phys. Rev. Lett., bf 103, 165002 (2009).
Y. Fukuda, "Ion acceleration via interaction of intense laser pulse with cluster-gas target", 31st European Conference on Laser Interaction with Matter (ECLIM), Budapest, Hungary, Sept. 2010.
Y. Fukuda et al., in Progress in Ultrafast Intense Laser Science VII, edt. K. Yamanouchi, Springer Verlag, p. 225, Berlin (2011).
E. Garin et al., Eur. J. Nucl. Med. Mol. Imaging 37, 453 (2010).
"Global Action Against Cancer", World Health Organization and International Union Against Cancer, (2005), ISBN 92-4-159314-8 (WHO)
C. Grignon et al., Nucl. Instr. Meth. A 571, 142 (2007).
Th. Haberer *et al.*, Radiotherapy and Oncology, 73 (2), 186 (2004).
D. Habs et al., Appl. Phys. B 93, 349 (2008).
D. Habs, in 440th WE Heraeus Seminar on *"Laser-driven particle and X-ray sources for medical applications"*, Frauenwörth, Sep. 13 – 17, 2009. http://www.ha.physik.uni-muenchen.de/veranstaltungen/workshops/
D. Habs, U. Köster; Appl. Phys. B 103, 501 (2011)
R. Hajima et al., Nucl. Instr. Meth. A608, S57 (2009).
R. Hajima, *High Flux and High Brilliance γ-ray Sources Based on Energy Recovery Linac*; http:/www.eli-np.ro/excecutive committee-meeting-april12-13.php (2010).
S. Hassfjell and M.W. Brechbiel, Chem. Rev. 101, 2019 (2001).

S. P. Hatchett *et al.*, Phys. Plasma 7, 2076 (2000).
B.M. Hegelich et al., accepted for publication in Nucl. Fus. (2011).
B. M. Hegelich *et al.*, Nature 339, 441 (2006).
A. Henig *et al.*, Phys. Rev. Lett. 103, 245003 (2009).
A. Jankowiak et al., Proceedings of LINAC 10, Tsukuba, Japan, Sept. 12-17, 2010, to appear. on http://www.JACoW.org/.
S. Kar *et al.*, Phys. Rev. Lett. 100, 105004 (2008).
N. Karavida and A. Notopoulos, Hippokratia 14, 22 (2010).
Y.A. Karelin et al., Appl. Radiat. lsot. 48, 1585 (1997).
Y. Kishimoto and T. Tajima, High Field Science, eds. T. Tajima, K. Mima, and H. Baldis (Kluwer, NY, 2000), pp. 83–96.
Y. Kishimoto, "Laser cluster interaction and ion acceleration aiming at the understanding of Kansai experiments", (2009) http://wwwapr.kansai.jaea.go.jp/pmrc_en/org/colloquium/
O. Klimo *et al.*, Phys. Rev. ST Accel. Beams 11, 031301 (2008).
F.F.(Russ) Knapp Jr.et al., J. Radioanal. Nucl. Chem. 263, 503 (2005).
U. Kneissl et al., J. Phys. G 32, R217 (2006).
R. Kodama et al., Nature 418, 933 (2002).
T. Kormoll et al., NIM A 626, 114 (2011).
S. Kraft, New J. Phys. 12, 085003 (2010).
V. V. Kulagin *et al.*, Phys. Rev. E 80, 016404 (2009).
X. Ledoux et al., Eur. Phys. J. A 27, 59 (2006).
Biol.
D.M. Lewis, Eur. J. Nucl. Med. Mol. Imaging 36, 1371 (2009).
M. Liepe et al., Proceedings of IPAC 10, Kyoto, Japan, May 23-28, 2010.
V.N. Litvinenko et al., IEEE Trans. Plasma Sci. 36, 1799 (2008).
B. C. Liu *et al.*, IEEE Transactions on Plasma Science 36 (4), 1854 (2008).
A. Macchi *et al.*, Phys. Rev. Lett. 94, 165003 (2005).
H.R. Maecke et al., J. Nucl. Med. 46 Suppl 1 , 172S (2005).
F. Mako and T. Tajima, Phys. of Fluids 27, 1815 (1984).
Maksimchuck *et al.*, Phys. Rev. Lett. 84,4108 (2000).
O.D. Maslov et al., Radiochemistry 48, 195 (2006).
K. Matsukado *et al.*, Phys. Rev. Lett. 91, 215001 (2003).
P. McKenna *et al.*, Phys. Rev. E 70, 034405 (2004).
P. McKenna *et al.*, Plasma Phys. Control. Fusion 49, B223 (2007).
Y. Miao et al., Clin. Cancer Res. 11, 5616 (2005).
M. Molls et al., in "The Impact of Tumor Biology on Cancer Treatment and Multidisciplinary Strategies" (eds.: M. Molls, P. Vaupel, C. Nieder, M. S. Anscher), 169, Springer-Verlag Berlin Heidelberg, (2009).
P. Mora, Phys. Rev. Lett. 90, 185002 (2003).
P. Mora, Phys. Rev. E 72, 056401 (2005).
G. A. Mourou *et al.*, Rev. Mod. Phys. 78, 591 (2006).
M. Murakami *et al.*, Proceedings (AIP, NY, 2008) p. 275.
T. Nakamura et al., Phys. Rev. Lett. 105, 135002 (2010).
P. von Neumann-Cosel et al., Phys. Lett. B 266, 9 (1991).
M. Passoni *et al.*, Phys. Rev. E 69, 026411 (2004).
M. Passoni and M. Lontano, Phys. Rev. Lett. 101, 115001 (2008).
F. Pegoraro and S. V. Bulanov, Phys. Rev. Lett. 99, 065002 (2007).

F. Pfeiffer *et al.*, Nature Physics 2, 258 (2006).
A. Pukhov, Phys. Rev. Lett. 86, 3561 (2001).
B. Qiao *et al.*, Phys. Rev. Lett. 102, 145002 (2009).
J. Raloff, ScienceNews 176, 16 (2009).
J.C. Reubi et al., J. Nuc. Med. 46, 67S (2005).
J.C. Reubi et al., Eur. J. Nucl. Med. 27, 273 (2000).
M.J. Rivard et al., Appl. Rad. Isotopes, 63, 157 (2005).
A. P. L. Robinson *et al.*, New J. Phys. 10, 013021 (2008).
L. Robson *et al.*, Nature Physics 3, 58 (2007), and refs. therein.
Bioconjugate Chem. 21, 811 (2010).
S. G. Rykovanov *et al.*, New J. Phys. 10, 113005 (2008).
D. Schardt et al., Rev. Mod. Phys. (2009) accepted.
Ch. Schiepers, *Diagnostic Nuclear Medicine*, Springer Verlag, Berlin (2006).
C.G. Schroer et al., Phys. Rev. Lett. 94, 054802 (2005).
H. Schwörer *et al.*, Nature 439, 445 (2006).
R. C. Shah *et al.*, Opt. Lett. 34, 2273 (2009).
R. A. Snavely *et al.*, Phys. Rev. Lett. 85, 2945 (2000).
L. Spencer *et al.*, Phys. Rev. E 67, 046402 (2003).
I. Stefanescu *et al.*, Phys. Rev. Lett. 98, 122701 (2007).
S. Steinke et al., Laser Part. Beams 28, 215 (2010).
S. Steinke et al., Contrib. Plas. Phys. 51, 444 (2011).
K. Sutherland et al., Radiol. Phys. Technol. 3, 16 (2010).
T. Tajima and F. Mako, Phys. Fluids 21, 1459 (1978).
T. Tajima and J. Dawson, Phys. Rev. Lett. 43, 267, (1979).
T. Tajima, J. Jpn. Soc. Ther. Radiol. Oncol. 9, suppl. 2, 83 (1997).
T. Tajima, Laser Driven Compact Ion Accelerator, US Patent 6,906,338B2 (filed: Jan 8, 2001; date of patent: June 14, 2005).
T. Tajima, D. Habs and X. Yan, Rev. Acc. Sci. and Tech., Vol. 2, p. 201 (2009).
S. Ter-Avetisyan *et al.*,, Phys. Rev. Lett. 96, 145006 (2006).
G. Tsakiris et al., New J. Phys. 8, 19 (2006).
H. Uusijärvi et al., J. Nucl. Med. 47, 807 (2006).
G.B.M. Vaughau et al., J. Sych. Rad. 18, 125 (2011)
V. A. Vshivkov *et al.*, Phys. Plasmas 5, 2727 (1998).
H.Y. Wang et al., Phys. of Plasm. 17, 113111 (2010).
H. Wang et al., arXiv:submit/0258702 [physics.plasm-ph] 2 jun (2011).
H.R. Weller et al., Prog. Part. Nucl. Phys. 62, 257 (2009).
S. C. Wilks *et al.*, Phys. of Plasm. 8, 542 (2001).
Ying Wu (Duke University), private communication, (2011).
http://www.nndc.bnl.gov/nudat2/
X. Q. Yan *et al.*, Appl. Phys. B 98, 711 (2009).
X. Q. Yan *et al.*, Phys. Plasmas, 16, 1 (2009).
L. Yin *et al.*, Phys. Plasmas 14, 056706 (2007).
A. Yogo *et al.*, Phys. Rev. E 77, 016401 (2007).
A. Yogo *et al.*, Appl. Phys. Lett. 94, 181502 (2009).

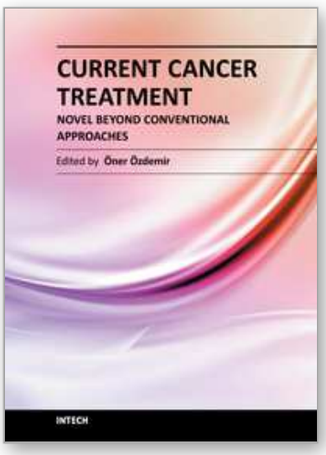

Current Cancer Treatment - Novel Beyond Conventional Approaches

Edited by Prof. Oner Ozdemir

ISBN 978-953-307-397-2
Hard cover, 810 pages
Publisher InTech
Published online 09, December, 2011
Published in print edition December, 2011

Currently there have been many armamentaria to be used in cancer treatment. This indeed indicates that the final treatment has not yet been found. It seems this will take a long period of time to achieve. Thus, cancer treatment in general still seems to need new and more effective approaches. The book "Current Cancer Treatment - Novel Beyond Conventional Approaches", consisting of 33 chapters, will help get us physicians as well as patients enlightened with new research and developments in this area. This book is a valuable contribution to this area mentioning various modalities in cancer treatment such as some rare classic treatment approaches: treatment of metastatic liver disease of colorectal origin, radiation treatment of skull and spine chordoma, changing the face of adjuvant therapy for early breast cancer; new therapeutic approaches of old techniques: laser-driven radiation therapy, laser photo-chemotherapy, new approaches targeting androgen receptor and many more emerging techniques.

INTECH
open science | open minds

InTech Europe
University Campus STeP Ri
Slavka Krautzeka 83/A
51000 Rijeka, Croatia
Phone: +385 (51) 770 447
Fax: +385 (51) 686 166
www.intechopen.com

InTech China
Unit 405, Office Block, Hotel Equatorial Shanghai
No.65, Yan An Road (West), Shanghai, 200040, China
中国上海市延安西路65号上海国际贵都大饭店办公楼405单元
Phone: +86-21-62489820
Fax: +86-21-62489821

IntechOpen